Torque from Solar Radiation Pressure Gradient During Eclipse

G.B. Sincarsin* and P.C. Hughes†
Institute for Aerospace Studies, University of Toronto, Toronto, Canada

A general formulation is developed for calculating penumbra solar-pressure-gradient torque. A literal expression for the dependence of light intensity on position is given and the three-dimensional gradient about any point of interest in the spacecraft is computed. Solar-gradient torques are studied, via numerical simulation, for both Earth-pointing and sun-pointing planar spacecraft in geostationary orbit. Both specularly reflecting and totally absorbing surfaces are considered. Eclipse conditions are identified for the following critical cases: 1) maximum solar-gradient pitch torque; 2) maximum solar-gradient roll torque; and 3) longest duration within penumbra. The maximum instantaneous torque and angular impulse from solar-gradient torque are compared with those arising from gravity-gradient torque and are shown to be significant for some spacecraft orientations. A comparison of equivalent center-of-mass-center-of-pressure offsets for solar-gradient and conventional solar torque indicates that solar-gradient torque may potentially become dominant for very large spacecraft. It is also argued that the symmetry present within an eclipse season permits an attitude control approach based on angular momentum storage.

Introduction

WHEN a spacecraft experiences solar eclipse by the Earth, a solar torque is generated by the nonuniform solar radiation pressure within penumbra. The variation in the light intensity within this partially lit transition zone between total darkness (umbra) and full sunlight causes even a "balanced" spacecraft to become "unbalanced." In the past, this solar-pressure-gradient torque (which does not depend on slight geometrical asymmetries for existence) appears to have attracted little attention. From dimension considerations, the conventional (full sunlight) solar torque varies as $p\ell^3$, where p is the solar pressure and ℓ a characteristic spacecraft dimension. Penumbral solar-gradient torque, however, varies as $(dp/dx)\ell^4$. Consequently, assuming geometrical similarity, solar-gradient torque will eventually dominate, for sufficiently large spacecraft (see, for example, the proposed 10-km "solar power satellite" in Fig. 1).

In this paper, a general (three-dimensional) expression for the gradient in solar pressure is derived by expanding the penumbral light intensity function in a first-order Taylor series. This enables the solar-gradient torque to be simulated numerically and permits the relative importance of conventional and solar-gradient torques to be assessed. A numerical comparison of gravity-gradient and solar-gradient torques also becomes convenient. In what follows, these comparisons are performed for both Earth-pointing and sun-pointing geostationary (planar) spacecraft possessing either specular reflecting or totally absorbing surfaces.

Penumbral Solar-Pressure-Gradient Force and Torque

Force and Torque: Neglecting the Pressure Gradient

Although Earth-orbiting spacecraft encounter radiation from a variety of sources (including the spacecraft itself) the major source remains direct photon radiation from the sun.[1]

The pressure caused by the impingement of this radiation upon a spacecraft surface is governed by its reflective properties. Here the incident radiation is assumed to be reflected, transmitted, and absorbed in the proportions ζ, τ and $1-\zeta-\tau$. Furthermore, χ of the reflected radiation is reflected specularly, while the remainder is reflected diffusely, and κ of the absorbed radiation is re-emitted diffusely. Now defining

$$\beta_1 = -\tfrac{1}{3}[(1-\chi)\zeta+\kappa(1-\zeta-\tau)] \qquad \beta_2=\chi\zeta$$

$$\beta_3=\tfrac{1}{2}(1-\chi\zeta-\tau) \tag{1}$$

the solar force and torque acting on the spacecraft surface-area element da shown in Fig. 2 are

$$df_s = 2H(\Lambda)(u_a/u_s)^2 p[\{\beta_1-\beta_2\cos\lambda\}\hat{n}+\beta_3\hat{u}_s]\cos\Lambda da \tag{2}$$

$$dg_s = \rho_s \times df_s \tag{3}$$

where ρ_s is the position vector from the point O to da. Λ is the (acute) angle between the incident radiation ($\hat{u}_s = u_s/u_s$) and the (outward) normal to da, $\hat{n}$. The Heaviside function $H(\Lambda)=1$, if da is exposed to the sun and $=0$ otherwise. In the absence of eclipsing, the solar pressure $p=P$, the solar

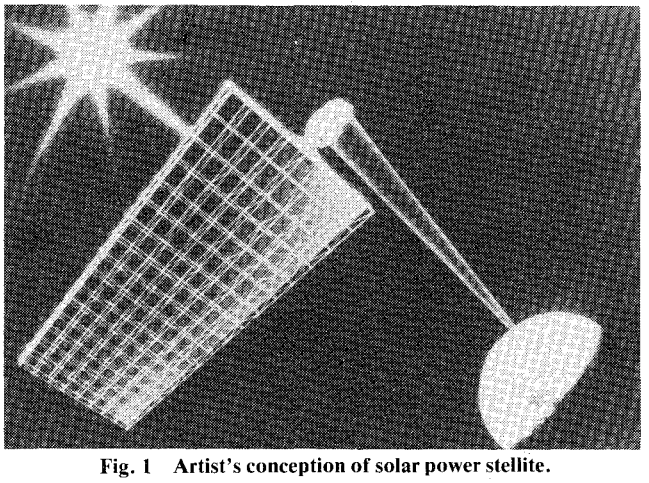

Fig. 1 Artist's conception of solar power stellite.

Presented as Paper 82-1612 at the AIAA Guidance and Control, Atmospheric Flight Mechanics, and Astrodynamics Conference, San Diego, Calif., Aug. 9-11, 1982; submitted Aug. 12, 1982; revision received March 22, 1983.

*Doctoral Candidate; presently, Senior Research Engineer, Dynacon Enterprises Ltd. Member AIAA.
†Professor. Associate Fellow AIAA.

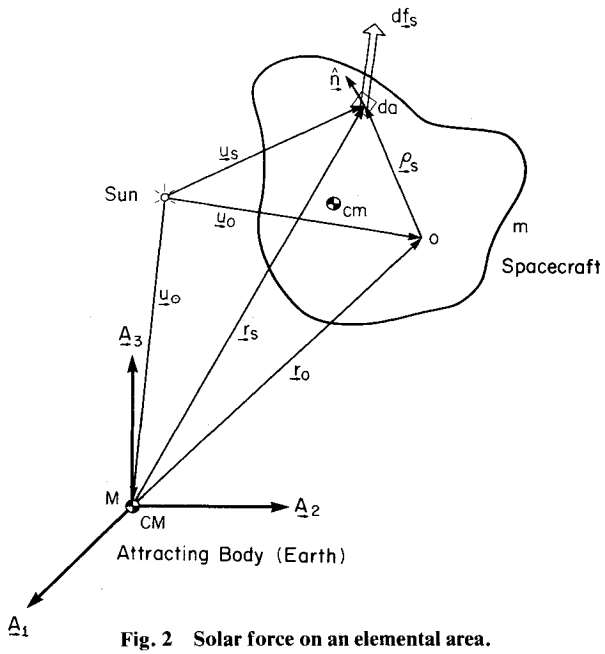

Fig. 2 Solar force on an elemental area.

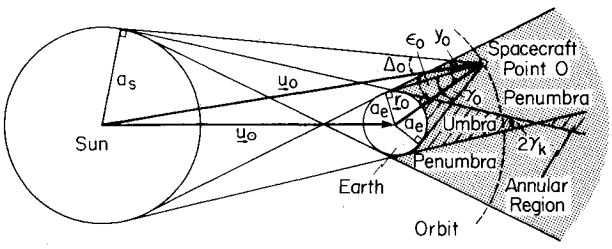

Fig. 3 Eclipse geometry.

constant ($P=4.51$ N/km^2 at the mean Earth-sun distance $u_a=1.496\times10^8$ km). The $(u_a/u_s)^2$ factor simply scales p to account for da not being exactly a distance u_a from the sun. Except for minor modifications, this is the solar-force model suggested by Georgevic.[2]

A simplifying assumption often made, and also adopted here, replaces the "true" direction of the incident radiation $\hat{u}_s$ in Eq. (2) with the sun-Earth vector $\hat{u}_\odot$. This eliminates the need to define a unique direction for the incident radiation striking each da. Essentially the (horizontal) parallax resulting from the orbital motion and the finite size of the spacecraft (58.13 and 0.021 arc·sec, respectively, for a 15-km spacecraft at geostationary altitude) are neglected. Also, the magnitudes of r_0 and ρ_s are neglected in comparison to that of $u_\odot$ in the factor scaling p. Simply, Eq. (2) becomes

$$df_s=2H(\Lambda)(u_a/u_\odot)^2 p[\{\beta_1-\beta_2\cos\Lambda\}\hat{n}+\beta_3\hat{u}_\odot]\cos\Lambda da \quad (4)$$

where, now

$$\cos\Lambda=-(\hat{u}_\odot\cdot\hat{n}) \quad (5)$$

and Eq. (3) remains unchanged.

The Intensity Function and the Solar Pressure Gradient

When a spacecraft experiences solar eclipse by the Earth, the solar pressure p is no longer a constant, but rather takes the form

$$p=P_p(u_s) \quad (6)$$

where $p(u_s)$, which we shall call the intensity function, depends on the eclipse region in which the spacecraft is located. The three possible eclipse regions for Earth-orbiting spacecraft are shown in Fig. 3. Only two, however, are practical: the umbra—the region of total darkness—and the penumbra—the partially lit transition zone between full sunlight and the umbra. (The annular eclipse region occurs beyond the orbital radius of the moon.) Now, the intensity function for the point O is unity in full sunlight, zero in umbra; and, in penumbra, it is given by Baker[3]:

$$p(u_0)=1-\left(\frac{\gamma_0}{\Delta_0}\right)^2\left[\frac{\alpha_0-\tfrac{1}{2}\sin2\alpha_0}{\pi}\right]-\left[\frac{\beta_0-\tfrac{1}{2}\sin2\beta_0}{\pi}\right] \quad (7)$$

where

$$\alpha_0,\beta_0=\cos^{-1}\left[\frac{\epsilon_0^2\pm(\gamma_0^2-\Delta_0^2)}{2\epsilon_0\gamma_0}\right] \quad (8)$$

and, from the geometry of Fig. 3,

$$\gamma_0=\sin^{-1}(a_e/r_0)\quad \Delta_0=\sin^{-1}(a_s/u_0)\quad \epsilon_0=\cos^{-1}(\hat{u}_0\cdot\hat{r}_0) \quad (9)$$

The geometry assumed to obtain $p(u_0)$ suffers two shortcomings. The first is that, even after the sun has "set" behind the Earth, some sunlight reaches the spacecraft because of diffraction and solar corona effects.[4,5] Consequently, a larger penumbra, containing more severe gradients in the solar radiation, results.[6] The second is that during eclipse the solar flux vector does not actually originate from the center of the sun, but rather its origin is an integral over the exposed area of the sun. (This introduces a maximum error of 0.5 deg for Earth-orbiting spacecraft.) An alternate, more complex form for $p(u_0)$, not employing the small angle approximations implicit in Eq. (7), is available[7]; however, the above two shortcomings are still not addressed. As such, the relative simplicity of Baker's approximate expression is favored from a computation standpoint and is the one adopted here. (Even more simplistic cylindrical-shadow models have found general acceptance.[8])

The intensity function $p(u_s)$ at an arbitrary spacecraft point can be expressed in terms of $p(u_0)$ by observing that

$$u_s=\rho_s+u_0 \quad (10)$$

($\rho_s\ll u_0$) and expanding about u_0 in a first-order Taylor series to obtain[9]

$$p(u_s)\cong p(u_0)+\rho_s\cdot\nabla p(u_0) \quad (11)$$

In spherical coordinates (see Fig. 4), the gradient of $p(u_s)$ (evaluated at $u_s=u_0$) is

$$\nabla p(u_0)=\frac{\partial p(u_0)}{\partial r_s}\hat{r}_0+\frac{1}{r_0}\frac{\partial p(u_0)}{\partial\theta_s}\hat{s}_0 \quad (12)$$

where $s_0=(\hat{u}_\odot\times\hat{r}_0)\times\hat{r}_0$, and $\theta_s=\cos^{-1}(\hat{u}_s\cdot\hat{r}_0)$ is the angle between r_s and the centerline of the umbral cone. [Note that $p(u_s)$ is independent of ϕ_s, as is reflected by the lack of a $\hat{q}_0=\hat{r}_0\times\hat{s}_0$ term in Eq. (12).] The partial derivatives in Eq. (12) take the form (with $\tau_s=r_s$ or θ_s)

$$\frac{\partial p(u_0)}{\partial\tau_s}=\frac{1}{\pi}\left(\frac{\gamma_0}{\Delta_0}\right)^2\left\{2\alpha_0\left[\frac{1}{\Delta_0}\Delta_{\tau_0}-\frac{1}{\gamma_0}\gamma_{\tau_0}\right]+\left[\sin2\alpha_0+\left(\frac{\Delta_0}{\gamma_0}\right)^2\sin\beta_0\right]\left[\frac{1}{\epsilon_0}\epsilon_{\tau_0}-\frac{1}{\Delta_0}\Delta_{\tau_0}\right]\right\} \quad (13)$$

with

$$\Delta_{r_0}=-(1/u_0)\tan\Delta_0\cos\epsilon_0 \qquad \Delta_{\theta_0}=(r_0/u_0)\tan\Delta_0\sin\epsilon_0$$
$$\epsilon_{r_0}=-(1/u_0)\sin\epsilon_0 \qquad \epsilon_{\theta_0}=1-(r_0/u_0)\cos\epsilon_0$$
$$\gamma_{r_0}=-(1/r_0)\tan\gamma_0 \qquad \gamma_{\theta_0}=0 \quad (14)$$

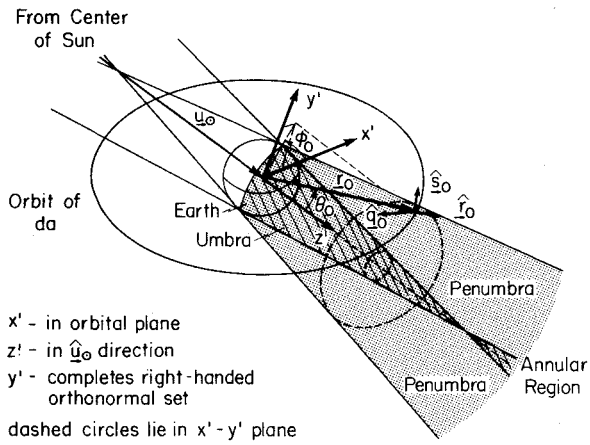

Fig. 4 Spherical coordinate system.

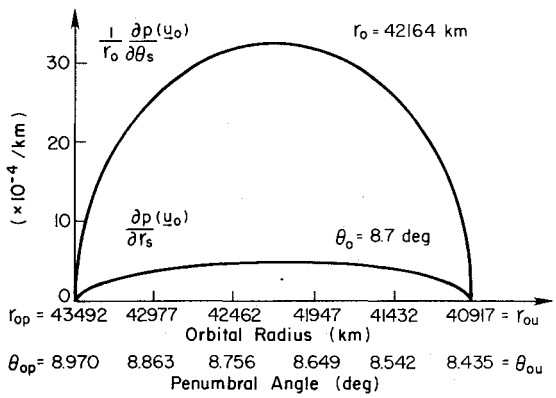

Fig. 5 Gradient components in the $\hat{r}_0$ and $\hat{s}_0$ directions.

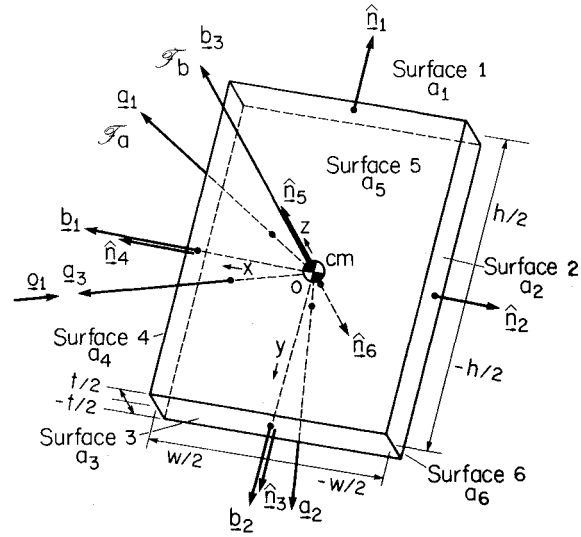

Fig. 6 Planar-form configuration.

Table 1 Physical parameters for the selected spacecraft designs

	Thin plate[12]	Rectangular beam[13]
Dimensions, $\times 10^3$ m		
h	13.1	26.7
w	4.93	1.9
t	0.21	1.5
Mass, $\times 10^6$ kg	18.06	24
Moments of inertia, $\times 10^{14}$ kg-m^2		
I_{11}	2.583	14.30
I_{22}	0.3665	0.1172
I_{33}	2.949	14.33

Their dependence as a function of spacecraft position within penumbra (they are zero otherwise) is illustrated in Fig. 5 by fixing $\theta_0 = 8.7$ deg for $\partial p(u_0)/\partial r_s$ (the midpoint angle for a geostationary spacecraft) and $r_0 = 42{,}164$ km for $\partial p(u_0)/\partial \theta_s$ (the orbital radius of a geostationary spacecraft). The remaining variable in each case (r_0 for the first, θ_0 for the second) is then varied from the penumbral boundary (r_{0p}, θ_{0p}) to the umbral boundary (r_{0u}, θ_{0u}).

Now, recalling Eqs. (3), (4), and (6), it is obvious that, while the first term in Eq. (11) simply yields the "conventional" solar pressure acting over the spacecraft, the second term results in what shall henceforth be called the penumbral *solar-pressure-gradient* torque. A one-dimensional model for this pressure gradient can be found in the literature[10]; however, to the authors' knowledge, the above general, three-dimensional result was not previously available.

Force and Torque: Including the Pressure Gradient

After substituting Eq. (6) [with $p(u_s)$ given by Eqs. (11-14)] into Eq. (4), and Eq. (4) into Eq. (3), integration over spacecraft area yields the total solar force and torque. The resultant solar-gradient force is an even function of ρ_s after integration and, hence, vanishes in the limit, for a spacecraft that is "balanced" (either by clever design or some semi-passive trim technique) such that its exposed surface area is symmetric about the spacecraft mass center. More important, from the viewpoint of attitude control, a balanced spacecraft experiences no conventional solar torque. The solar-gradient torque (an odd function of ρ_s after integration), however, does not vanish even for a perfectly balanced spacecraft. The question becomes, for a slightly "unbalanced" spacecraft: Can solar-gradient torque dominate conventional solar torque? Also of interest is the importance of this torque relative to other environmental torques, especially gravity-gradient torque, which can rival conventional solar torque at geostationary altitude. These issues are addressed in what follows.

Solar-Gradient Torque Magnitude

Description of Study

The planar spacecraft shown in Fig. 6 (several proposed designs for solar power satellites and futuristic orbiting antennas have essentially this shape[11]) is chosen for the purposes of comparison because the conventional solar torque for this configuration is ideally zero, thus permitting a direct comparison of solar-gradient and gravity-gradient torque, and because the inertia parameters for a variety of spacecraft, varying from thin plates to cubes, can be considered. The two spacecraft studied here via numerical simulation are a thin plate[12] and a beamlike[13] craft with an almost square cross-section about the pitch axis b_2 (see Table 1). Both specularly reflecting and totally absorbing surfaces are considered. The former yields perturbing forces predominantly in the orbital plane, while the latter is a source for out-of-plane perturbing forces. (The finite thickness of the spacecraft results in some minor out-of-plane forces, even for specular reflection.)

A geostationary orbit is assumed, with the spacecraft in either an Earth- or a sun-pointing orientation (the pitch axis is parallel to the orbit normal). No gravitational coupling of the attitude and orbit is permitted, and while solar forces are computed they are not applied to the orbital equations of motion. (The solar force and torque expressions and the motion equations governing the spacecraft shown in Fig. 6 are documented in Ref. 9.) As a consequence the orbit remains unperturbed. No attitude motion is permitted beyond that applied by an *ideal controller* to keep the largest surface area

of the craft always pointing directly towards either the Earth or the sun. That is, the controller compensates perfectly for all environmental torques.

For the chosen spacecraft, gravity-gradient and solar-pressure torques are dominant.[14] Their relative importance depends upon the type of disturbing torque being considered—nominal or incremental. The disturbing torque is said to be "nominal" when the spacecraft attitude is unperturbed, while an incremental disturbing torque (the change in torque per degree change in attitude) occurs when the attitude is perturbed. Nominal "conventional" solar-pressure torque dominates gravity-gradient torque because, for the chosen spacecraft orientations (ones generally accepted for solar power satellites), no nominal gravity-gradient torque exists. (Only exception: When the spacecraft is sun-pointing a nonzero gravity-gradient pitch torque exists that may exceed the solar pressure torque; however, for the thin plate of Table 1, the magnitudes of these two torques are the same.[14]) Furthermore, whereas the pitch gravity-gradient torque is periodic, so that momentum can be temporarily stored and then later "dumped" each orbit, the solar-pressure torque on a sun-pointing spacecraft is "constant" over several orbits.

The incremental gravity-gradient torque for the chosen orientation exceeds the incremental solar-pressure torque by approximately two orders of magnitude.[14] Still, solar pressure causes the second most important incremental disturbing torque. It must also be recognized that once the nominal attitude for the chosen spacecraft is perturbed, the resulting gravity-gradient torque is destabilizing about pitch and roll. As the major source for the original perturbation is the nominal solar-pressure torque, it is essential that this torque be controlled—the better one counteracts the solar torque, the smaller the change in attitude and the lower the control effort required to counteract the resulting gravity-gradient torque. It is, therefore, most useful to assess the significance of solar-gradient torques by direct comparison with gravity-gradient and conventional solar torques.

To permit direct comparison, the gravity-gradient and solar-pressure torques (conventional and solar-gradient) are computed, but not applied to the attitude motion equations. Hence the torques (and forces) in what follows are those which would have to be applied by an actual control system to maintain either an Earth- or sun-pointing orientation. Interestingly, because of the eclipse syzygy, these two orientations, characteristic of most Earth-orbiting spacecraft, yield similar results.

Critical Eclipses

As a consequence of eclipse geometry, solar-gradient torques are pitch-dominant during the equinoxes; they are roll-dominant at the beginning and end of each eclipse *season* (for a geostrationary spacecraft, two 7-week seasons exist each year, one "straddling" the vernal equinox and the other the autumnal equinox). A third critical eclipse of interest is the one producing the longest duration within the penumbra (~24 min for a geostationary spacecraft). This condition might be expected to yield the largest angular impulse from solar-gradient torque, an expectation further supported by the fact that during this time the largest roll torque experienced is 95% of its possible maximum. We shall present results, therefore, for the vernal equinox case and the maximum duration case (following the vernal equinox).

For the vernal equinox case, the orbital motion of the spacecraft and sun are started in phase at the vernal equinox, with the spacecraft on the illuminated side of the Earth. As a result, after 12 mean solar hours, the spacecraft is at the point A shown in the insert to Fig. 7 ($\lambda \cong 180.5$ deg, where λ is the true longitude of the spacecraft orbit relative to the vernal equinox). The sun is approximately 0.2 deg above the equatorial plane and, because the shadow moves with the sun, the spacecraft actually passes through the shadow at a slight angle (hence, while the pitch torque is 99% of maximum, a small roll torque is also induced).

For the maximum duration case, the orbital motions of the spacecraft and sun are started out of phase (the first in the equatorial plane and the second in the ecliptic plane). The spacecraft again begins its orbital motion on the illuminated side of the Earth so that after 12 sidereal hours it is at the point A ($\lambda \cong 200$ deg); however, now the spacecraft just clears the umbra when at A (Fig. 8 insert). The sun's orbital motion is started near the end of the vernal-equinox season, such that after this same 12-h period the sun, Earth, and spacecraft are aligned.

Maximum Instantaneous Torques: Solar-Gradient vs Gravity-Gradient

Figures 7 and 8 depict the cases (spacecraft design, surface reflectivity, pointing orientation, and critical eclipse) that

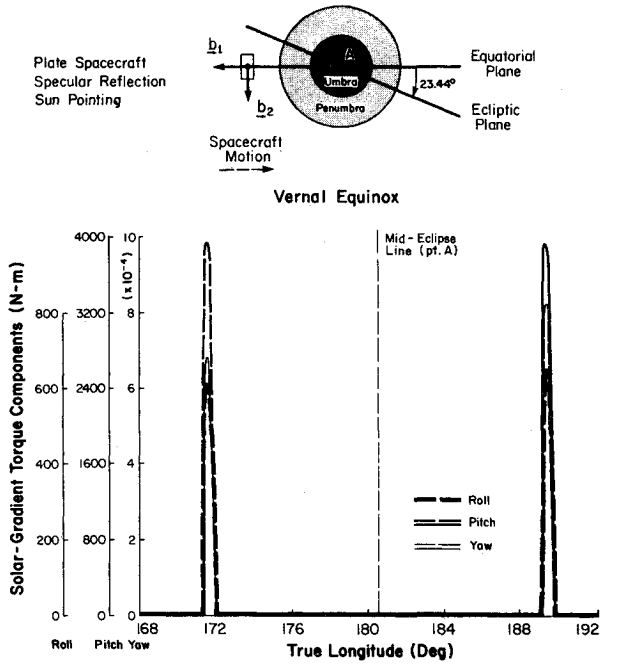

Fig. 7 Solar-gradient torques at vernal equinox.

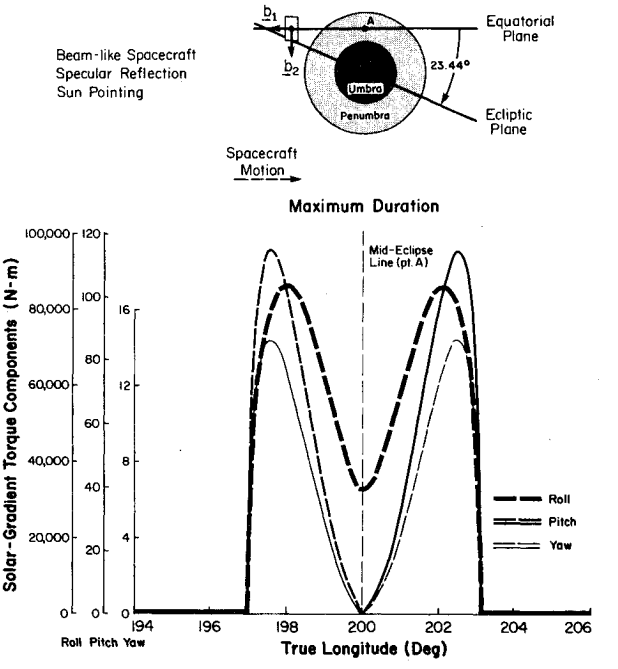

Fig. 8 Solar-gradient torques at maximum duration.

Table 2 Maximum instantaneous solar-gradient torque components, N-m

	Vernal equinox case					Maximum duration case			
Earth-pointing									
Torque	Plate		Beam		Torque	Plate		Beam	
Component	Specular	Absorbed	Specular	Absorbed	Component	Specular	Absorbed	Specular	Absorbed
Roll	621	313	2032	1132	Roll	25,526	12,947	83,421	43,895
Pitch	3726	1900	436	305	Pitch	952	482	111	64.2
Yaw	0.63	41	38	174	Yaw	1.55	436	113	1726
Sun-pointing									
Torque	Plate		Beam		Torque	Plate		Beam	
Component	Specular[a]	Absorbed	Specular	Absorbed	Component	Specular	Absorbed	Specular	Absorbed
Roll	637	320	2084	1040	Roll	25,592	12,842	83,684	42,947
Pitch	3853	1926	448	224	Pitch	979	492	114	57.6
Yaw	8×10^{4}	6.97	3×10^{-4}	0.81	Yaw	0.35	73.2	0.14	8.34

[a] Figure 7. [b] Figure 8.

Table 3 Magnitudes of angular impulses caused by solar-pressure-gradient torque components, N-m-s)

	Vernal equinox case					Maximum duration case			
Earth-pointing									
Torque	Plate		Beam		Torque	Plate		Beam	
Component	Specular	Absorbed	Specular	Absorbed	Component	Specular	Absorbed	Specular	Absorbed
Roll	5.2×10^{4}	3.2×10^{4}	1.8×10^{5}	9.8×10^{4}	Roll	1.3×10^{7}	6.7×10^{6}	4.4×10^{7}	2.3×10^{7}
Pitch	3.0×10^{5}	2.1×10^{5}	3.9×10^{4}	2.8×10^{4}	Pitch	3.6×10^{5}	1.8×10^{5}	4.3×10^{4}	2.4×10^{4}
Yaw	4.0×10^{1}	3.8×10^{3}	3.3×10^{3}	1.6×10^{4}	Yaw	4.2×10^{2}	1.7×10^{5}	3.5×10^{4}	6.6×10^{5}
Sun-pointing									
Torque	Plate		Beam		Torque	Plate		Beam	
Component	Specular	Absorbed	Specular	Absorbed	Component	Specular	Absorbed	Specular	Absorbed
Roll	5.8×10^{4}	3.1×10^{4}	1.7×10^{5}	7.7×10^{4}	Roll	1.3×10^{7}	6.5×10^{6}	4.4×10^{7}	2.3×10^{7}
Pitch	3.7×10^{5}	1.9×10^{5}	3.8×10^{4}	1.9×10^{4}	Pitch	3.6×10^{5}	1.8×10^{5}	4.4×10^{4}	2.2×10^{4}
Yaw	5.6×10^{-2}	5.4×10^{2}	2.3×10^{-2}	6.2×10^{-1}	Yaw	1.3×10^{2}	2.7×10^{4}	5.5×10^{1}	3.3×10^{3}

yield the maximum instantaneous solar-gradient pitch and roll torque, respectively. The magnitudes of the torque components are plotted, with dashed lines denoting a negative torque about either the roll $\boldsymbol{b}_1$, the pitch $\boldsymbol{b}_2$, or the yaw $\boldsymbol{b}_3$ axis (see Fig. 6). Table 2 provides a complete set of data for the cases studied. In all cases the dominant torque component is either roll or pitch. Furthermore, these components are not significantly different for Earth- and sun-pointing spacecraft because of the similarity in geometrical alignment at eclipse. Yaw torque, however, is somewhat greater for Earth-pointing spacecraft. The roll and pitch components are also approximately half as great for an absorbing surface as for a specular one. Again the yaw component deviates from the pattern and is much greater for an absorbing surface.

For both chosen orientations gravity-gradient torque exists about the pitch axis only:

$$g_{gg2}=3\omega_c^2(I_3-I_1)\sin\Theta\cos\Theta \tag{15}$$

Here Θ is the pitch angle, ω_c is the orbital rate, and I_1 and I_3 are the principal inertias about $\boldsymbol{b}_1$ and $\boldsymbol{b}_3$ ($\mathfrak{F}_b$ is a body-fixed frame). In truth, $g_{gg2}\equiv 0$ for the Earth-pointing orientation since $\Theta\equiv 0$. For the sun-pointing orientation, the maximum gravity-gradient torque for the plate spacecraft (at $\Theta=\pi/4$) is 2.91×10^{5} N-m and for the beam spacecraft is 2.17×10^{4} N-m. From Table 2, these torques are at least two orders of magnitude larger than their solar-gradient counterparts. This observation is reversible, however, for as the spacecraft design becomes more inertially balanced about pitch [i.e., let t approach w in Fig. 6 so that $(I_3-I_1)\to 0$], the solar-gradient torque is essentially unchanged (hw a constant) and will eventually dominate.

Angular Impulse: Solar-Gradient vs Gravity-Gradient

The angular impulse associated with a solar-gradient torque component g_{sgi} (expressed in $\mathfrak{F}_b$) is

$$M_{sgi}=\frac{1}{\omega_c}\int_{\lambda_1}^{\lambda_2} g_{sgi}\,d\lambda \tag{16}$$

where λ_1 and λ_2 are the true longitude at entry into penumbra and of point A (recall Figs. 7 and 8). The resulting M_{sgi} are shown in Table 3. Now, the angular impulse (over one-quarter of the period of Θ) of the only nonvanishing gravity-gradient component can be approximated by

$$M_{gg2}=\frac{1}{(\omega_c-\omega_s)}\int_0^{\pi/2} g_{gg2}\,d\Theta \tag{17}$$

where g_{gg2} is given by Eq. (15), and ω_s is the mean orbital rate of the sun. Again, for an Earth-pointing spacecraft, $M_{gg2}\equiv 0$ and solar-gradient torques dominate. Furthermore, as before, the impulses from gravity-gradient torques are substantially larger than their solar-gradient counterparts. Compare the M_{gg2} for the plate (4.0×10^{9} N-m-s) and the beam (3.0×10^{8} N-m-s) spacecraft with those in Table 3. However, as with the maximum instantaneous torque, for an inertially balanced spacecraft, the impulses from solar-gradient torques will dominate.

From a control standpoint, solar-gradient torques basically pose an angular momentum storage problem. The pitch and yaw torques are *symmetrical* on a *per-eclipse* basis (see Figs. 7 and 8), while the roll torque is symmetrical on a *per-eclipse-season* basis (another maximum duration case occurs near the beginning of the vernal equinox eclipse season with the roll

Table 4 Equivalent cm-cp offsets

Estimated "conventional" solar torque cm-cp offsets, m

ρ_c	Plate Specular	Plate Absorbed	Beam Specular	Beam Absorbed
Roll	85.2	170.3	173.6	347.1
Pitch	197.2	394.4	76.0	152.0

Solar-pressure-gradient torque cm-cp offsets, m

Vernal equinox case

Earth-pointing

ρ_g	Plate Specular	Plate Absorbed	Beam Specular	Beam Absorbed
Roll	1.1	1.1	4.5	4.5
Pitch	6.5	6.6	0.97	1.2

Sun-pointing

ρ_g	Plate Specular	Plate Absorbed	Beam Specular	Beam Absorbed
Roll	1.1	1.1	4.6	4.6
Pitch	6.6	6.6	0.99	0.99

Maximum duration case

Earth-pointing

ρ_g	Plate Specular	Plate Absorbed	Beam Specular	Beam Absorbed
Roll	45.1	45.8	187.9	188.4
Pitch	1.7	1.7	0.25	0.28

Sun-pointing

ρ_g	Plate Specular	Plate Absorbed	Beam Specular	Beam Absorbed
Roll	45.1	45.2	189.3	191.7
Pitch	1.7	1.7	0.26	0.26

torque reversed). It is possible, therefore, to store the angular impulse over the first portion of each symmetrical period and "dump" it during the second, using, for example, reaction wheels. (The fact that the sun changes position during eclipse introduces a slight asymmetry into the torque histories and the small residual angular momentum has to be eventually dumped.) For an Earth-pointing orientation, where nominally zero gravity-gradient torque exists, solar gradient torques would control wheel sizing. More important, regardless of which attitude orientation is maintained, roll and yaw solar-gradient torques are dominant because, for $\boldsymbol{b}_2$ perpendicular to the orbital plane, no gravity-gradient torque nominally exists about either roll or yaw.

Relative Importance of Pressure-Gradient and Conventional Solar Torques

Recall that conventional solar torque ($\boldsymbol{g}_{sf}$) occurs in full sunlight and does not depend on a solar pressure gradient for its existence. In penumbra, it still exists but is reduced by the decrease in light intensity reaching the spacecraft and is augmented by the introduction of the solar-pressure-gradient torque ($\boldsymbol{g}_{sg}$). The total solar torque acting on the spacecraft is then

$$\boldsymbol{g}_{sp} = \mathrm{p}(\boldsymbol{u}_{\oplus})\,\boldsymbol{g}_{sf} + \boldsymbol{g}_{sg} \tag{18}$$

where the point O is taken to be the spacecraft mass center [recall $0 < \mathrm{p}(\boldsymbol{u}_{\oplus}) < 1$ in penumbra]. The question becomes: Can solar-gradient torque ever dominate that in full sunlight ($g_{sg} > g_{sf}$)? Or, more likely: Can solar-gradient torque cause the net torque in the penumbra to exceed that in full sunlight ($g_{sp} > g_{sf}$)?

The answer to the first question is obviously in the affirmative for the spacecraft design under study, since $\boldsymbol{g}_{sf} \equiv 0$ and $\boldsymbol{g}_{sg} \neq 0$. In reality, however, some conventional solar torque will exist. If the conventional and solar-gradient torque act in the same direction then

$$g_{sg} > [1 - \mathrm{p}(\boldsymbol{u}_{\oplus})]\, g_{sf} \tag{19}$$

is sufficient to guarantee $g_{sp} > g_{sf}$. If they appose one another then the required condition becomes

$$g_{sg} > [1 + \mathrm{p}(\boldsymbol{u}_{\oplus})]\, g_{sf} \tag{20}$$

Obviously Eq. (19) is the limiting case of primary practical interest as it marks the point at which solar-gradient torques makes a significant contribution to the solar torque model for a given spacecraft.

If $\boldsymbol{g}_{sf}$ can be viewed as being caused by some equivalent center-of-mass-center-of-pressure (cm-cp) offset, that is,

$$\boldsymbol{g}_{sf} = \boldsymbol{\rho}_c \times \boldsymbol{f}_{sf} \tag{21}$$

where $\boldsymbol{\rho}_c$ is the position vector from the center of mass to the equivalent "center of pressure" (this is not always definable for a general three-dimensional structure) and $\boldsymbol{f}_{sf}$ is the solar force in full sunlight, then the maximum possible g_{sf} is $\rho_c f_{sf}$. Therefore condition (19) becomes

$$\rho_g > [1 - \mathrm{p}(\boldsymbol{u}_{\oplus})]\, \rho_c \tag{22}$$

where $\rho_g = g_{sg}/f_{sf}$.

To assess the significance of Eq. (22) for our two sample spacecraft geometries, it is necessary to estimate ρ_c. This is done by extrapolating from current spacecraft of similar shape and applying geometric similarity. The Communications Technology Satellite (CTS—renamed Hermes),[15] with a surface area of approximately 21.1 m^2 (86% of this attributed to the solar arrays), is chosen here. Assuming specular reflection and incident radiation normal to the array surface (i.e., aligned with $\boldsymbol{b}_3$), the solar force is 1.9×10^{-4}N. As CTS is essentially 1.3×16.8 m and experiences a solar torque of 1×10^{-5} N-m about pitch and 2×10^{-5} N-m about roll, ρ_c for pitch is

$$\rho_{cp} = 4.0 \times 10^{-2}\, w \tag{23}$$

and for roll,

$$\rho_{cr} = 6.5 \times 10^{-3}\, h \tag{24}$$

Application of Eqs. (23) and (24) to the corresponding dimensions for the two chosen spacecraft designs produces the estimated offsets shown in Table 4.

It is straightforward to compute ρ_g (see Table 4) from the torques shown in Table 2. The radial force component in full sunlight just prior to eclipse (not shown here) is used to estimate f_{sf}. (Consequently the ρ_g in Table 4 are slightly overestimated.) Now, realizing that the maximum instantaneous solar-gradient torques occur when $\mathrm{p}(\boldsymbol{u}_{\oplus}) \cong \frac{1}{2}$, the ρ_c and ρ_g in Table 4 should be tested using the inequality

$$\rho_g > \tfrac{1}{2}\rho_c \tag{25}$$

For the maximum duration eclipse, condition (25) is true for the roll torque components of both spacecraft (except for the plate with an absorbing surface), regardless of the pointing orientation. This comparison of effective cm-cp offsets indicates that as planned spacecraft grow in size their large

surface areas will magnify the importance of the small solar pressure gradient in the penumbra to yield a solar torque which may potentially become dominant, especially if "conventional" offsets can be minimized to a greater degree than geometric extrapolation of present-day spacecraft would suggest. For instance, based on a conventional solar torque model, a 25-m cm-cp offset (along the b_2 axis) has been predicted for a thin-plate spacecraft similar to the one described in Table 1.[14] (The spacecraft has the same dimensions; however, the inclusion of a central transmitting antenna results in slightly different inertial properties.) This represents a reduction of over 70% in the smallest extrapolated ρ_c cited in Table 1.

Conclusions

For very large spacecraft solar-pressure-gradient torque can become significant and can produce a solar torque in penumbra greater than that experienced in full sunlight. It dominates gravity-gradient torque, both in magnitude and angular impulse, for some spacecraft.

Solar-gradient torque is roll-dominant at the beginning and end of each eclipse season; it is pitch-dominant during the equinoxes. Because of the similarity in geometrical alignment at eclipse, only yaw torque is significantly different for Earth-pointing and sun-pointing spacecraft. Also, only the yaw torque deviates from the pattern that the torque components are approximately twice as great for a specular reflecting surface as for an absorbing one.

An attitude control approach based on angular momentum storage is possible because of the symmetry inherent in each eclipse season. In this regard, for a sun-pointing geostationary spacecraft oriented perpendicular to the equatorial plane, the out-of-plane (roll and yaw) solar-gradient torque components cause greatest concern. If the spacecraft is Earth-pointing, the in-plane (pitch) component also becomes important.

As conventional solar torques are reduced by better geometric "balancing" of spacecraft, and as spacecraft continue to become larger in size, solar-gradient torque will clearly become increasingly important.

Acknowledgment

This work was sponsored by the Natural Sciences and Engineering Research Council of Canada under Grant A4183.

References

[1] Harris, M. and Lyle, R., "Spacecraft Radiation Torques," NASA SP-8027, Oct. 1969.

[2] Georgevic, R.M., "The Solar Radiation Pressure on the Mariner 9 Mars Orbiter," *Astronautica Acta,* Vol. 18, 1973, pp. 109-115.

[3] Baker, R.M., *Astrodynamics—Applications and Advanced Topics,* Academic Press, New York, 1967, pp. 186-198.

[4] Moore, R.C. and Shilling, G.F., Rand Memorandum No. 4557-PR, 1965.

[5] Link, F., *Eclipse Phenomena in Astronomy,* Springer-Verlag, New York, 1969.

[6] Gersten, R.H., "A Method for Determining Satellite Illumination During an Eclipse by Earth," *The Journal of Astronautical Sciences,* Vol. 14, Sept.-Oct. 1966, pp. 199-201.

[7] Wertz, S., *Spacecraft Attitude Determination and Control,* D. Reidel, Holland, 1978.

[8] Cappellari, J.O., Valez, C.E., and Fuchs, A.J., "Mathematical Theory of the Goddard Trajectory Determination System," NASA TMX-71106, April 1976.

[9] Sincarsin, G.B., "Gravitational Orbit-Attitude Coupling and Penumbral Solar-Gradient Torques for Very Large Spacecraft," University of Toronto, Institute for Aerospace Studies, Toronto, Canada, Rept. No. 265, 1982.

[10] Etkin, B., "Attitude Stability of Articulated Gravity-Oriented Satellites. Part 1—General Theory and Motion in Orbital Plane," University of Toronto, Institute for Aerospace Studies, Toronto, Canada, Rept. No. 89, 1962.

[11] Woodcock, G.R., "Solar Satellites—Space Key to Our Power Future," *Astronautics & Aeronautics,* Vol. 15, July/Aug. 1977, pp. 30-43.

[12] Glaser, P.E., "The Potential of Satellite Solar Power," *Proceedings of the IEEE,* Vol. 65, Aug. 1977, pp. 1162-1176.

[13] Oglevie, R.E., "Attitude Control of Large Solar Power Satellites," AISS Paper 78-1266, Palo Alto, Calif., Aug. 7-9, 1978, pp. 571-578.

[14] *AIAA Guidance and Control Conference Proceedings,* "Space-Based Solar Power Conversion and Delivery Systems," NASA, MSFC, Contract NAS8-31308, Second Interim Report Study, Vol. II, *Engineering Analysis of Orbital Systems,* June 30, 1976.

[15] Franklin, C.A. and Davison, E.H., "A High Power Communications Technology Satellite for the 12 and 14 GHz Bands," AIAA 4th Communications Satellite Systems Conference, AIAA Paper 72-580, Washington, D.C., April 1972.